Optimal design of steel exoskeleton for the retrofitting of RC buildings via genetic algorithm

Computers and Structures 299 (2024) 107396

Contents lists available at ScienceDirect

Computers and Structures

journal homepage: www.elsevier.com/locate/compstruc

Optimal design of steel exoskeleton for the retrofitting of RC buildings via genetic algorithm

Jana Olivo, Raffaele Cucuzza *, Gabriele Bertagnoli, Marco Domaneschi

Politecnico di Torino, Department of Structural, Geotechnical and Building Engineering, Corso Duca Degli Abruzzi, 24, Turin, 10128, Italy

ARTICLE INFO

Keywords:
Exoskeletons
Seismic retrofit
Optimization
Genetic
Finite element
Steel

ABSTRACT

In recent decades, steel exoskeletons have gathered significant attention as a seismic retrofitting technique for existing structures. The design methods proposed so far are focused on the identification of the system's overall parameters through simplified models. Although these methodologies provide helpful guidance at the preliminary design stage, they do not consider aspects such as the distribution of the exoskeletons and sizing of their components. To overcome these limitations, an optimization process based on the Genetic Algorithm is proposed in this paper to identify the optimal exoskeleton number and spatial arrangement, and to determine the optimal size of their constituent elements. The algorithm aims to minimize the weight of the retrofit solution while keeping the whole existing structure in the elastic field and ensuring the structural verification of the exoskeleton's elements. The analyses have been conducted using a finite-element code with an Open Application Programming Interface, which allows the models to be handled through automatic routines. The proposed optimization tool has been applied to several case studies, considering two different layouts for the exoskeletons. Finally, the effectiveness of the retrofit method has been demonstrated, and the proposed optimization tool has been able to significantly reduce the weight and cost of the intervention.

1. Introduction

Several countries are characterized by building stock whose construction dates back to the economic expansion that occurred after the World War II, when the structural design guidelines often underestimated or did not consider seismic hazard. Additionally, these buildings have nowadays passed their expected lifespan, presenting durability issues and strength loss [1,2]. The combination of vulnerability and seismicity takes on specific relevance, especially in areas characterized by significant seismic hazard. [3,4].

Simultaneously, the same buildings may also exhibit poor energy performance, as constructions contribute to more than one-third of greenhouse gas emissions [5]. Moreover, as remarked in [6], the lack of aesthetic and functional consideration of the post-war buildings represents another crucial aspect that should be addressed. Thus, a structural, energetic, and architectural renovation of a substantial portion of the building stock requires urgent attention [7].

Especially for large-scale renovation plans of urban areas where a huge number of buildings require massive retrofit interventions, the traditional retrofitting approaches lead to limited structural, architectonic and energetic restoration rates with significant economic costs and disruptions to the community [8]. Examples of these are the organizational limits related to the interruption of ordinary life and the temporary relocation of the inhabitants [9,10] or the suspension of production activities hosted in industrial buildings [11–13]. Moreover, technical challenges arise from the limited range of conventional solutions that may fail to address specific case requirements or economic issues due to the high costs of interventions [14].

Traditional retrofitting techniques for masonry, reinforced concrete, and other building typologies, are particularly interesting and provide great benefits for seismic improvement of existing structures [15,16]. Moreover, many alternatives based on the installation of earthquake-resistant devices are available on the market and are presented in the literature [17–19], as well as in regulations [20,21].

However, local retrofitting techniques such as RC, steel, or FRP and steel jacketing, as well as bracing systems or shear walls, do not ensure the proper performance of operational and logistic activities during the retrofitting interventions (e.g., hospitals, factories, schools, and other strategic facilities) [22,23]. Additionally, many strengthening solutions do not serve the aesthetic or energetic renovation purpose of buildings.

* Corresponding author.
E-mail address: raffaele.cucuzza@polito.it (R. Cucuzza).

https://doi.org/10.1016/j.compstruc.2024.107396
Received 30 December 2023; Accepted 28 April 2024
Available online 7 May 2024

With the aim of overcoming the limitations of these approaches, alternative solutions, like exoskeleton systems, have gained considerable attention. Being inspired by biomimicry [24,25], they represent a non-invasive and efficient solution, that augments the building's stiffness and resistance to lateral forces, thereby significantly unloading the structure from seismic actions [26,27].

Exoskeletons can have either two or three-dimensional arrangements of their components [28], being oriented perpendicular or parallel to the building's façade.

Several authors investigated their seismic energy dissipation capacity, as they can enhance the building's structural behavior either by accommodating dissipative devices [29–31] or by providing extra-stiffness to the system.

Service downtime and functionality loss can be minimized since only the external facade of the building is affected during the consolidation, reducing the intervention's costs and operational times [23,32]. Interference with existing structural components is also limited, as it is confined to the connection points between the anchorage joints of the existing structure and the exoskeleton. By adopting this approach, independent foundations of the exoskeleton system are often designed due to the important base shear attracted by the strengthening system.

In the context of urban renewal and regeneration, this retrofitting system is suitable for a holistic intervention [33,34], through the creation of a double skin of the structure [35,36]. Therefore, a combined approach in terms of structural safety, energetic performance, and aesthetic value, can be performed [37,38].

It is also worth noting that the use of metallic materials, especially steel, provides a lightweight and highly resistant solution, while reducing transportation and installation inconveniences. Metallic structures offer a compelling advantage in construction due to their prefabrication and dry assembly, which reduce construction times. Additionally, their reversible nature, and the possibility of dismantling, recycling, and reusing, contribute to a promising low environmental impact of the solution. Hence, this technique has the potential to adhere to the Life Cycle Thinking principles, while reducing construction times and costs [39].

Nevertheless, a retrofit with exoskeletons is not suited for every case. Free space around the building's perimeter is a fundamental requirement for the installation of the new foundations and their interference with existing substructures should be taken into account. Furthermore, if the preservation of the façade is required, exoskeletons are not a viable alternative [40].

Only a few authors addressed the design process of exoskeletons, mainly focusing on the determination of overall stiffness, mass, and damping values of the system. This is usually accomplished through the simplification of the building-exoskeletons assembly as two coupled SDoF (Single-Degree-of-Freedom) systems. Although this approach has been proven useful, the performance of the solution is heavily influenced by factors such as the morphology and sizing of the exoskeletons, along with the amount and distribution of the connections with the existing structure.

The retrofitting design procedures by adopting exoskeletons proposed by various authors exhibit several common aspects. These approaches are mainly outlined as a series of steps, that can be summarized in the following way:

- **Step #1**: Definition of the design targets. The targets include floor displacements, inter-storey drifts, shear forces, and floor accelerations [41]. According to the Performance Based Design principle, these parameters must be chosen to limit the damage of structural and non-structural elements at the Life Safety Limit State [42].
- **Step #2**: Multi-Degree-of-Freedom (MDoF) to Single-Degree-of-Freedom (SDoF). This step is related to the simplification of the coupled system (i.e. base structure and strengthening system) as two coupled SDoF systems, by means of a rigid link, or a Hooke spring with a certain stiffness [43].
- **Step #3**: Evaluation of the design parameters intended as the overall mass [29] and stiffness [7] of the retrofitting system. If dissipative devices are introduced in the intervention, an additional parameter is considered to account for the damping of the device [40].

Even though the benefits derived from the described approach have been proven, all these procedures, based on simplified models, do not provide an automatized approach for the final optimal design of the exoskeleton system [44]. In other words, the member sizing and optimal placement of the strengthening systems are always obtained by following engineering common practices or design guidelines based on previous experience [45].

This study is focused on addressing this limitation through the introduction of an optimal tool based on a metaheuristic algorithm [46,47]. Especially for complex engineering problems subjected to proper mathematical constraints, such algorithms exhibit high efficiency in handling non-linear [48,49], non-convex and high computationally demanding combinatorial problems [50,51] characterized by discontinuous solution space [52]. Metaheuristics are versatile in various domains as they require little to no prior knowledge of the tackled problem. Their primary objective is to get close to the optimal solution, finding good, feasible solutions in an acceptable timescale [53].

Among all these stochastic techniques that appeared in Literature, population-based algorithms are the most adopted due to their promising converge capability and robustness [54]. The main advantage of these algorithms is their potential parallelism, meaning that a population can simultaneously explore the search space in multiple directions because multiple offspring of the population act like independent agents [55].

In this work, the optimal amount and placement of the exoskeletons as well as the optimal sizing of their constituent elements have been achieved by implementing an adapted version of the well-known Genetic Algorithm [56]. The optimization process aims to attain the lightest possible solution while satisfying two crucial constraints. The first constraint is intended for maintaining the entire existing structure within the elastic field by imposing a maximum allowable inter-storey drift (limiting the damage to non-structural elements like partition walls and façade). The second restriction guarantees the compliance of the exoskeleton elements with the structural verifications. The implementation of this tool in the design process results in lightweight and cost-efficient exoskeletons, successfully achieving the targeted outcomes and rendering this solution feasible for a retrofitting intervention.

Furthermore, two different exoskeleton layouts have been analyzed, i.e., orthogonal and parallel to the building's façade. Through the investigation of three different case studies, the efficiency of the optimal retrofitting strategy has been tested on real-world inspired buildings. Each of these has been retrofitted by adopting both exoskeleton layouts, providing interesting insights into the resulting structural behavior. Finally, comparisons between the non-retrofitted configurations and the retrofitted ones have been conducted aiming to give an engineering interpretation of the numerical results pointed out by the optimization process.

This paper presents the following organization: in Section 2, the details of the designed optimization tool are presented, by the mathematical formulation of the Objective Function and the step-by-step explanation of the algorithm employed. In Section 3, the considered exoskeleton layouts and the case studies are defined. Section 4 presents the results, addressing the optimization tool performance and the overall structural behavior, and summarizes some overall design principles. The conclusions of the work are presented in Section 5.

2. Optimization framework

In this section, the framework of the optimization process is described. The mathematical formulation of the Objective function as well

as the boundary constraints of the optimization problem are introduced. Finally, a detailed description of the operators involved in the optimization tool is provided by emphasizing the difference with the standard version of the GA.

2.1. Mathematical formulation of the objective function

An optimization tool based on GA, with problem-specific adaptations, is proposed in this work to address the design of the exoskeletons, including the quantity and placement, as well as the sizing of their elements. The Objective Function (OF), the Constraints and Penalties, and the Design Variables (DV) are defined by the Eqs. (1)-(9), which introduce the mathematical framework of the optimization process.

$$\textbf{min } F(\mathbf{x}) = \left[N_{Ex} \cdot \rho \sum_{j=1}^{N_{El}} A_j \cdot l_j \right] \cdot \phi_1(D_i) \cdot \phi_2(S_j) + \phi_3(N_{Ex}) \quad (1)$$

$$\mathbf{x} = [\overbrace{x_1, \dots, x_i, \dots, x_n}^{\text{Topology DV}}, \overbrace{x_{n+1}, \dots, x_{n+j}, \dots, x_{n+m}}^{\text{Size DV}}] \quad (2)$$

Subjected to:

$$x_i = \begin{cases} 0 \\ 1 \end{cases} \quad ; \quad x_{n+j}^{lower} < x_{n+j} < x_{n+j}^{upper} \quad (3)$$

$$D_i = \frac{\delta_i}{\delta_{allowable}} < 1 \qquad \forall\, i = 1, \dots, N_{nodes} \quad ;$$

$$\delta_{allowable} = \frac{H_{storey}}{\beta} \quad (4)$$

$$S_{j,1} = \frac{N_{Ed}}{\chi_a \cdot N_{Rd}} + \sqrt{\left(k_{ay} \cdot \frac{M_y^{Ed} + N_{Ed} \cdot e_{N_y}}{\chi_{LT} \cdot M_y^{Rd}} \right)^2 + \left(k_{az} \cdot \frac{M_z^{Ed} + N_{Ed} \cdot e_{N_z}}{M_z^{Rd}} \right)^2} < 1 \quad (5)$$

$$S_{j,2} = \frac{V_{Ed}}{V_{pl,T,Rd}} < 1 \quad ; \quad V_{pl,T,Rd} = \left[1 - \frac{\tau_{t,Ed}}{(f_y/\sqrt{3})/\gamma_{M0}} \right] V_{pl,Rd} \quad (6)$$

In these, N_{Ex} is the total number of exoskeletons, ρ is the steel weight per unit volume, N_{El} is the number of elements of a single exoskeleton, and A_j and l_j are the cross-sectional area and length of the single element j, respectively.

As presented in Eq. (1), the Objective Function aims at exoskeletons' weight minimization. This weight is modified by three penalties: the first two correspond to the imposed constraints while the third one corresponds to constructability issues, as explained in this Section.

Two constraints are imposed. The first one, defined in Eq. (4), represents a maximum inter-storey drift limit. This limit corresponds to the threshold beyond which damage occurs in the building, considering both the structural and the non-structural elements (like partition walls or finishing). The limit is $\delta_{allowable}$, defined as a ratio between the storey height H and a factor β, the latter being determined empirically and taking a value of 600 [57,58]. Therefore, D_i, which is the ratio between the inter-storey drift δ_i of the *i-th* node of the existing structure, and the allowable limit $\delta_{allowable}$, should be lower than one. δ_i is the difference between the displacement of the *i-th* node and the displacement of the corresponding node in the floor directly below it. This condition is imposed for all the column-beam nodes of the existing building (N_{nodes}).

The second constraint is defined in Eqs. (5) and (6). It is related to the structural verifications of steel elements defined in the European standard regulation (EC3) [59], concerning the bearing capacity of the exoskeletons' elements. Specifically, Eq. (5) refers to the combined bending and axial compression, accounting for buckling, according to EC3 6.3.3.(6.61-6.62) and Eq. (6) refers to combined shear force and torsional moment, according to EC3 6.2.7.(6.25) and (6.28). Therefore, $S_{j,n}$, which are the Demand-Capacity Ratios of the *j-th* exoskeleton element according to the structural verification n, should be lower than one. This is imposed for all the elements of each exoskeleton.

A penalty system is employed to incorporate the constraints in the Objective Function (Eq. (1)). The three adopted penalties are defined in Eqs. (7), (8) and (9).

$$\phi_1 = \sum_{i=1}^{N_{nodes}} D_i^{inf} \quad (7)$$

$$\phi_2 = \sum_{j=1}^{N_{Ex}} \sum_{i=1}^{N_{el}} S_{i,j}^{inf} \quad ; \quad S_{i,j} = max \left\{ S_{i,j,1} \,;\, S_{i,j,2} \right\} \quad (8)$$

$$\phi_3 = \alpha \cdot N_{Ex} \quad (9)$$

The first penalty, ϕ_1 defined in Eq. (7), is related to the first constraint (Eq. (4)), regarding the maximum allowable inter-storey drift. To determine the value of this penalty, the ratios D_i, between the inter-storey drift of each node of the existing building (δ_i) and the allowable limit ($\delta_{allowable}$), are calculated. Then, the ratios that have a value bigger than 1, meaning, those which do not comply with the imposed limitation, called D_i^{inf}, are added to obtain ϕ_1. In this way, both the total amount and the severity of the violations for a certain configuration are considered.

A similar approach is followed for the determination of the second penalty, ϕ_2 defined in Eq. (8). In this case, the Demand-Capacity Ratios (DCR) of the exoskeleton's members, defined in Eqs. (5) and (6) are considered, and the values $S_{i,j}$ bigger than 1 ($S_{i,j}^{inf}$) are computed. Both penalties ϕ_1 and ϕ_2 multiply the weight in the OF (Eq. (1)), and these assume values equal to 1 if none of the constraints are violated for any node or element.

A third penalty ϕ_3 is defined in Eq. (9), to take into consideration the disadvantages of adopting a solution with a large number of exoskeletons. It derives from the fact that the free space around the building usually hosts specific activities and enhances the accessibility to the building. Thus, the building's activities might suffer from the occupation of this space with exoskeletons. Additionally, a larger amount of exoskeletons can imply higher transportation costs, assembly and erection time, and risks. Lastly, by reducing the number of exoskeletons, also the amount of columns of the existing building hosting connections with the retrofitting system, is reduced. Thus, ϕ_3 is defined as the total number of exoskeletons N_{Ex} by a factor α preliminary assumed equal to 10, and added to the OF already multiplied by ϕ_1 and ϕ_2, so that the algorithm slightly prefers solutions with fewer exoskeletons.

The design variables vector, also called chromosomes of the single individual, defined in Eq. (2) is constituted by two groups of variables. The first ones, called *Topology DVs*, from x_1 to x_n, allow the eventual activation of the exoskeleton at that specific position. If $x_i = 1$, an exoskeleton is placed in the i^{th} position, instead, if $x_i = 0$ that position is left free. In this way, the number of exoskeletons and their positions along the building's perimeter are univocally determined at each iteration according to the code of chromosome.

The second group of variables in Eq. (2), called *Size DVs*, go from x_{n+1} to x_{n+m}, where m is the number of different members, characterized by proper geometric and mechanical section properties, that constitute the exoskeleton system. In this case study, having all the buildings three stories, m is assumed equal to 8. The adopted grouping strategy of the cross-section is presented in Fig. 4 and it corresponds to the columns, beams, and bracings of the exoskeletons, and the links between the retrofitting system and the building. These variables represent the steel cross sections chosen for each element. In this case study, a list of Circular Hollow sections (CHS) composed of 150 different cross sections, according to the European code EN10219-2, is chosen since they are widely used in similar professional practice applications.

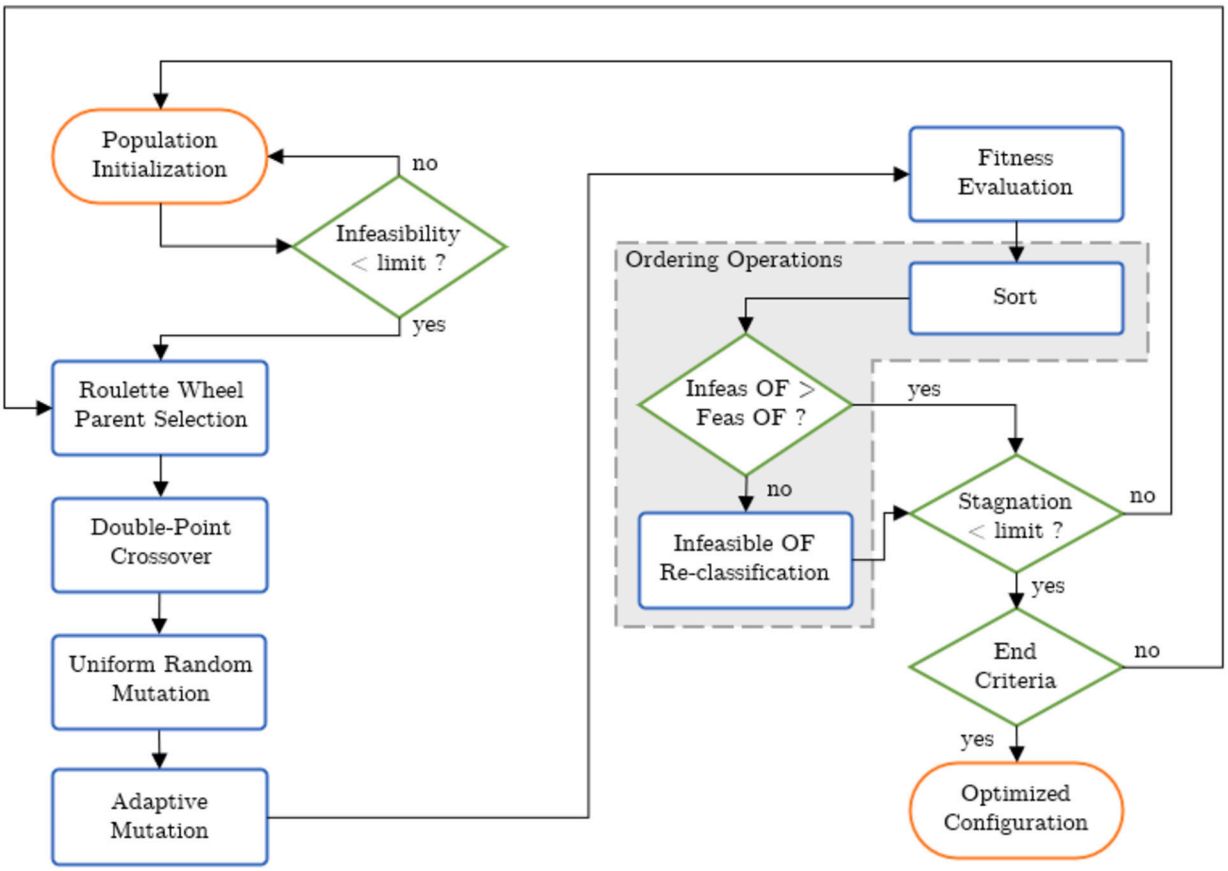

Fig. 1. Flowchart of the adapted Genetic Algorithm employed for the optimization process.

2.2. Employed algorithm

The optimization process herein adopted is based on the Genetic Algorithm, introducing problem-specific adaptations to ensure good performance for the investigated class of problem. The steps of the optimization process are presented in the flowchart in Fig. 1.

Once the initial population has been initialized, through the random definition of the chromosome and the assignment of the fitness value for each individual, the number of infeasible individuals in the population is evaluated. If at least one individual is feasible, i.e., it satisfies all the established constraints, an iterative process begins. Following the traditional strategies of the Genetic Algorithm, the parent selection is performed through the Roulette Wheel [60], and a number of children equal to that of the parents is generated by a Double Point Crossover [61].

Two distinct strategies are employed for the mutation. In the first one, a uniform random mutation is performed [62]: every variable of every individual is a candidate for mutation, with a predefined probability. A bit-flip mutation is employed for the *Topology DVs*, while a section is randomly chosen from the list in the predefined range for the *Size DVs*.

If certain individuals have significantly better OFs than others, these will have a higher probability of being chosen in the parent selection. This can lead to the emergence of *repeated individuals* in subsequent populations, which share the same chromosome as their predecessors [63]. An approach designed for the specific case study is proposed for these cases, introducing a second mutation strategy. The *Adaptive Mutation* is applied to all the groups of identical individuals, maintaining one original individual for each group and slightly mutating the others. In this way, the predominance of these outstanding solutions in the population is maintained, while augmenting the exploitation and introducing a refinement procedure. For this process, there is no probability associated with the mutation, instead, all the repeated individuals but one, for each repeated chromosome, will be mutated.

The strategy, illustrated in Fig. 2, starts by dividing the chromosome into nine parts that are potential targets for mutation. Then, each part is assigned a probability of 1/9, and only one of them is selected for mutation. The first part comprises all the *Topology DVs*, and its mutation involves rearranging the existing exoskeletons while keeping their amount constant, but changing their positions. The remaining eight parts are constituted each by a Size DV. If one of these is chosen for mutation, another section is selected from the section list within a predefined proximity of the current one. The potential sections to be selected are given by one of the two sections with immediately smaller cross-sections than the current one, or one of the two with immediately larger cross-sections.

After completing the mentioned steps, the fitness of the children is assessed through Multimodal Spectral Analyses. Eigenvectors are selected to perform the analyses, and the modal responses are combined by the Complete Quadratic Combination (CQC) [64] method. The number of modes taken into account allows to get 85% participating mass for Ux, Uy, and Rz, and ranges from 120 to 220 modes depending on the case study. The analyses are conducted using SAP2000 OAPI [65], a tool that enables the automatic model generation, modification, and analysis, as well as the retrieval of the results, controlled by a Matlab algorithm [66].

Once the fitness of each individual has been assessed, a set of *Ordering Operations* takes place, presented in Fig. 3. These operations sort the parents and children of the *i-th* iteration to obtain the new population, to be used in the iteration $i + 1$.

Individuals are categorized as feasible or infeasible according to the boundary constraints introduced by Eqs. (4)-(6) and the corresponding penalties are computed following Eqs. (7)-(9). Simultaneously, individuals can be unique or repeated, with the latter occurring when two or

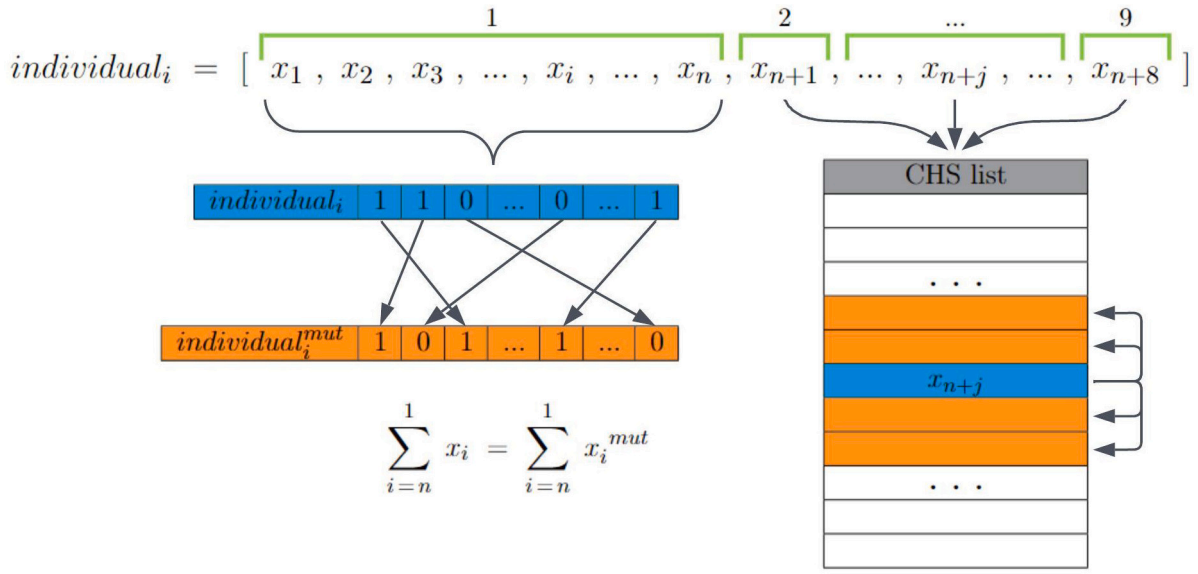

Fig. 2. Adaptive Mutation Strategy applied to the repeated individuals of the population.

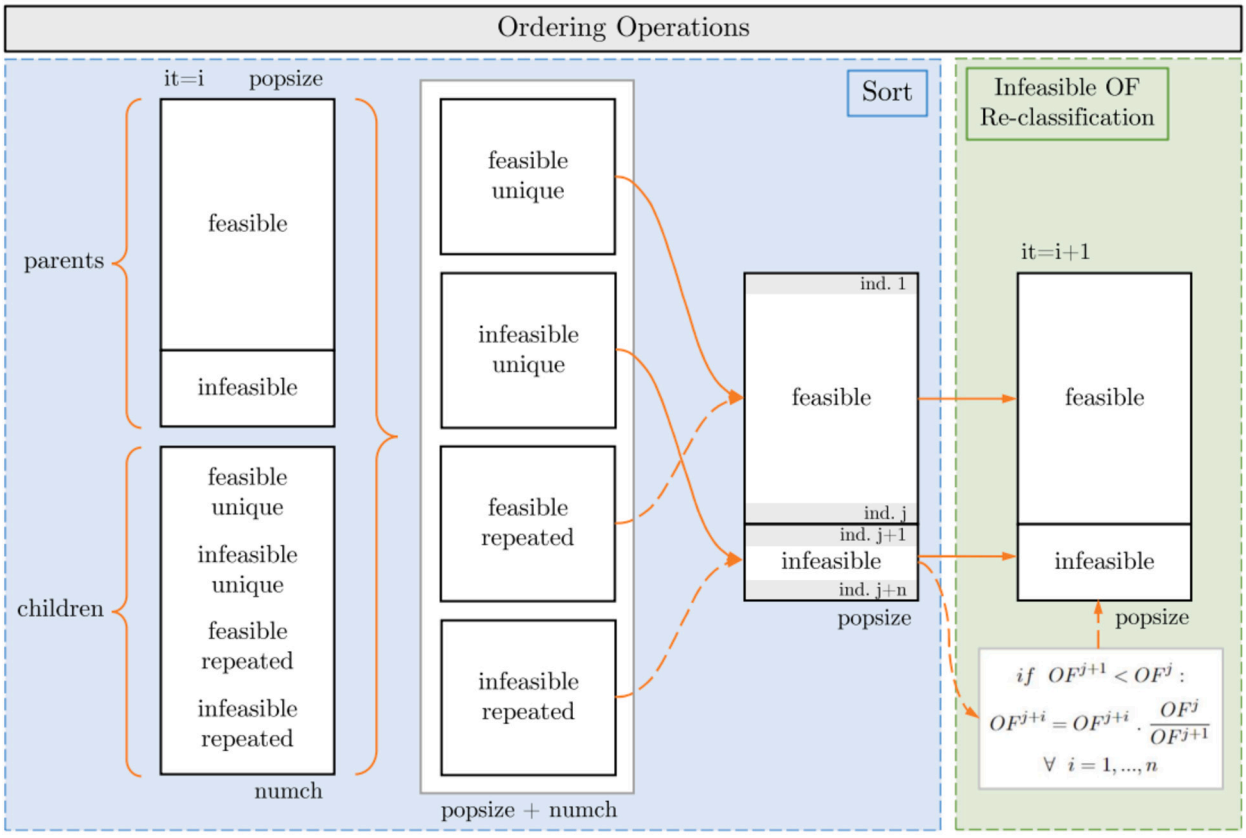

Fig. 3. Sort and Infeasible OF Re-classification strategies for the assembly of the population.

more individuals have the same OF. This is possible when the *Topology DVs* are mutated during the *Adaptive Mutation*. If the mutated individual remains feasible, both the weight and penalties will remain the same, resulting in both, the mutated and the original individual, having the same OF.

In the described scenario, the repeated individuals of a certain OF are sorted from lower to higher values of $D_i^{max} + S_{j,n}^{max}$. Here, D_i^{max} is the ratio between the maximum inter-storey drift among all the nodes of the existing structure (δ_i^{max}), and the maximum allowable limit ($\delta_{allowable}$). And $S_{j,n}^{max}$ is the higher DCR among all the elements of the exoskeletons, corresponding to the critical structural verification n, being n equal to 1 (Eq. (5)) or 2 (Eq. (6)). The motivation behind this strategy is that, at equality of weight, the solution that achieved a higher inter-storey drift control or lower DCR of the exoskeletons, performs better.

After each individual of the population has been categorized as feasible or infeasible, and as unique or repeated, the population for the following iteration is assembled, as shown in Fig. 3. The first part of the new population is constituted by feasible individuals, however, a predetermined percentage of infeasible individuals is intentionally inserted to enhance the algorithm's exploration, specifically 10% of the popula-

Table 1
Definition of the Case Studies (CS) and their corresponding optimization parameters.

	CS 1	CS 2	CS 3	CS 4	CS 5	CS 6
building	Square-shaped		L-shaped		U-shaped	
exoskeletons	orthogonal	parallel	orthogonal	parallel	orthogonal	parallel
variables	16 + 8	12 + 8	34 + 8	30 + 8	52 + 8	48 + 8
population size	100	100	200	200	250	250
max iterations	100	100	200	200	200	200

tion. Unique individuals are preferred during the assembly, but if there are not enough to meet the required percentage, repeated individuals are included in the order in which they were sorted.

If the OFs of the infeasible individuals are lower than that of the worst feasible individual, an OF re-classification is performed for the infeasible individuals, as depicted in Fig. 3. Specifically, the OFs of all infeasible individuals are multiplied by a certain factor, given by the ratio between the fitness of the worst feasible individual (OF^j) and the fitness of the best infeasible one (OF^{j+1}). In this way, the rank deriving from the infeasible individuals sort is maintained, while they all have higher OF values than the worst feasible ones.

Finally, at the end of each iteration, the best individual of the current iteration is confronted with the ones of the previous iterations. If there has been no improvement in the solution over successive generations (10% of the predefined maximum number of iterations), a stagnation strategy is implemented. For this strategy, the entire population is re-initialized, except for the best 3% of the individuals of the current generation, that are maintained. The stopping criterion is given by the maximum number of iterations, defined specifically for each case study depending on its complexity.

The described optimization tool will be applied to various case studies to assess its efficiency and robustness in identifying the optimal solution for each specific problem. The case studies, which differ in complexity level and amount of variables, are described in detail in the subsequent section.

3. Case studies

Six case studies are presented in this section. They are related to three simple Reinforced Concrete buildings, each one retrofitted with the two different exoskeleton layouts under study, i.e. orthogonal or parallel to the building façades. Table 1 specifies the building and exoskeleton layouts that constitute each case study. The parameters of the optimization process, selected for each case study, in terms of number of variables, population size, and number of iterations, are also presented.

Starting from CS1 up to CS6, an increasing complexity concerning the total number of elements and feasible exoskeleton positions (i.e. number of DVs) as well as in-plant irregularity is addressed. According to this, the exploration and exploitation capability of the algorithm has been set by increasing proportionally the number of population size and maximum iterations.

3.1. Exoskeleton layouts

The exoskeleton layouts considered for this study are depicted in Fig. 4. They are non-dissipative steel frames, entirely constituted by standard Circular Hollow Sections (CHS) realized with steel S355. The cross-sections for the exoskeleton elements are outputs of the optimization process and are arranged as depicted in Fig. 4. The steel profiles are chosen from a standard section list composed of 150 different cross-sections according to the European code EN10219-2. All the exoskeletons constituting the intervention for a case study employ the same cross-sections. It means that all exoskeleton used for a given building are exactly the same.

CHS profiles are chosen due to their inertia which is high and equal in both principal directions. This aspect is an advantage in cases, like this one, where exoskeleton elements need high buckling resistance. Exoskeletons not only have to withstand significant forces in their in-plane direction, but are also subjected to out-of-plane seismic forces generated by the movement of the building and their own mass. In particular, the orthogonal exoskeleton layout presents higher instability issues.

The exoskeletons work as truss bracing systems. Hinges are adopted to represent the connections between the steel elements with the exception of elements *X4* and *X8* for the orthogonal direction and elements *X8* for the parallel direction which are fully restrained.

In the orthogonal layout, the external columns suffer higher instability issues than the internal ones that work together with the R.C. columns of the building. In the parallel layout, all steel columns are coupled to reinforced concrete ones with multiple connections exhibiting lower levels of stress. In the orthogonal layout, transverse stiffness to reduce the buckling length of the external column may be provided at each storey by the full restraint given to elements *X4* and *X8* or by adding two horizontal ties (tensed ropes) connecting the external points of elements *X4* to other exoskeletons or to the main structure.

Both layouts present advantages and disadvantages with specific regard to their structural behavior and architectonic aspects. Orthogonal exoskeletons require more free space around the building to be installed, while parallel exoskeletons, being positioned closer to the building's façade, become a suitable option when the surrounding available space is limited.

Nevertheless, parallel structures cover the whole bay where they are applied, being more invasive and limiting the accessibility to the building and the functionality of the openings (windows). Focusing on their structural behavior, parallel exoskeletons demonstrate greater efficiency within the proposed case studies. Section 4 undertakes a more thorough examination of their functioning.

3.2. Geometrical model and load definition of non-retrofitted structures

The three buildings under study are reinforced concrete framed structures without vertical shear walls or bracings realized with C35/45 concrete, and Fe 450c steel rebars. The beams and columns are fully restrained to each other, and the columns are fully restrained to the foundation.

The choice of the geometry, as well as material for concrete and rebars, is done to make the investigated case studies similar to the typical non-retrofitted configuration of real-world buildings that are not compliant to seismic design requests.

Nevertheless, the buildings are not real structures, as they are obtained by replication of a regular module, which is a 3 by 3 bay framed structure of 3 storey. Each bay is 5 meters long, while the floor height is 4 meters, consequently, the base module is a square of 15 meters wide and 12 meters height.

The first structure under analysis is exactly one square-shaped base module (Fig. 5.a), while the subsequent two are L-shaped (Fig. 5.b) and U-shaped (Fig. 5.c), respectively. These last two are selected in order to account for some in-plan irregularities and to expand the range of

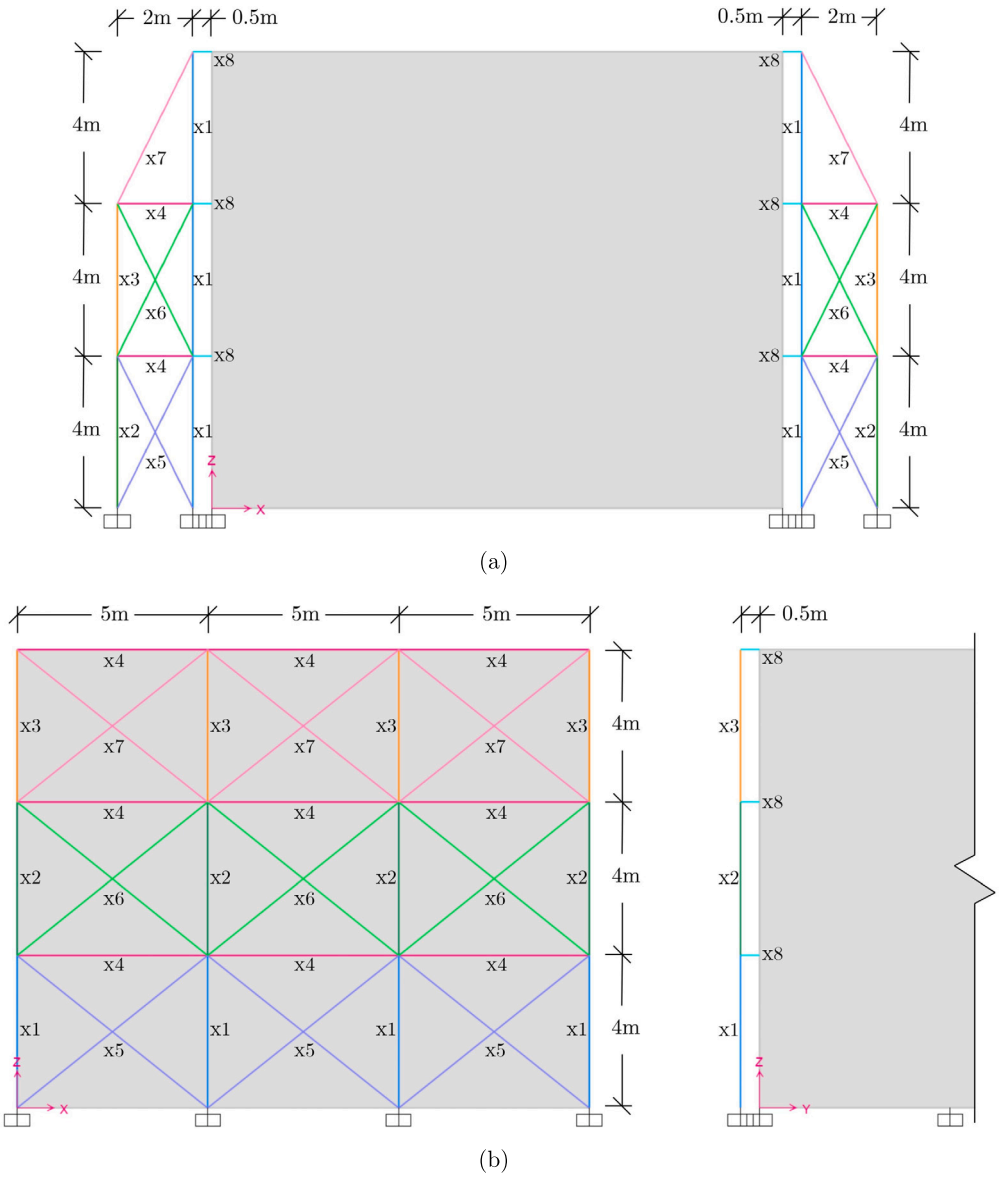

Fig. 4. Views of (a) Orthogonal and (b) Parallel Exoskeletons, and *Size DVs*.

potential exoskeleton positions, subsequently increasing the difficulty and computational burden associated with the optimization process.

The plan of the three buildings and all the potential exoskeletons positions are presented in Fig. 5, both orthogonal (blue) and parallel (orange) to the building's façade.

The original buildings have been designed with outdated standards, using the structural scheme of strong-beam and weak-column type. They are safe under static loads but they do not match seismic requirements as can usually happen in real buildings designed in the past. The authors chose to have almost all the elements (i.e. beams and columns) characterized by largely unsafe Demand-Capacity Ratio in order to justify the choice of exoskeletons as retrofitting solutions instead of traditional local reinforcement approaches, that may be suitable in less severe conditions.

The main characteristics of the original buildings are presented in Table 2 in terms of top displacement, maximum inter-storey drift (ISD), seismic mass ($G_1 + G_2 + G_3 + \psi_2.Q$), maximum Demand-Capacity Ratio (DCR), position of the center of mass (CM) and of the center of stiffness (CK), and the eccentricities e_x and e_y between them.

Table 2
Main characteristics of the unretrofitted buildings.

	squared-shaped	L-shaped	U-shaped
top displacement [mm]	44.4	46.3	43.7
max. ISD [mm]	18.79	19.32	18.20
seismic mass [ton]	796.2	2945.3	5071.8
max. DCR	2.082	2.154	2.114
CM position (x ; y) [m]	7.50 ; 7.50	11.55 ; 19.05	21.18 ; 22.50
CK position (x ; y) [m]	7.50 ; 7.50	11.28 ; 18.66	20.61 ; 22.50
eccentricity e_x [m]	0.00	0.27	0.57
eccentricity e_y [m]	0.00	0.39	0.00

The vertical loads are modeled considering 3 kN/m^2 as dead load G_1 representing the slabs selfweight, a permanent load G_2 of 2 kN/m^2 representing screed and partition walls, a permanent load G_3 of 10 kN/m for the building's façade, applied on the external beams, and a live load Q of 3 kN/m^2. Such loads, except for the one corresponding to the façade, are applied on the principal beams, aligned in the x direction.

The effect of the seismic action is simulated coherently with the elastic response spectrum of an Italian South-East City (Foggia), for the

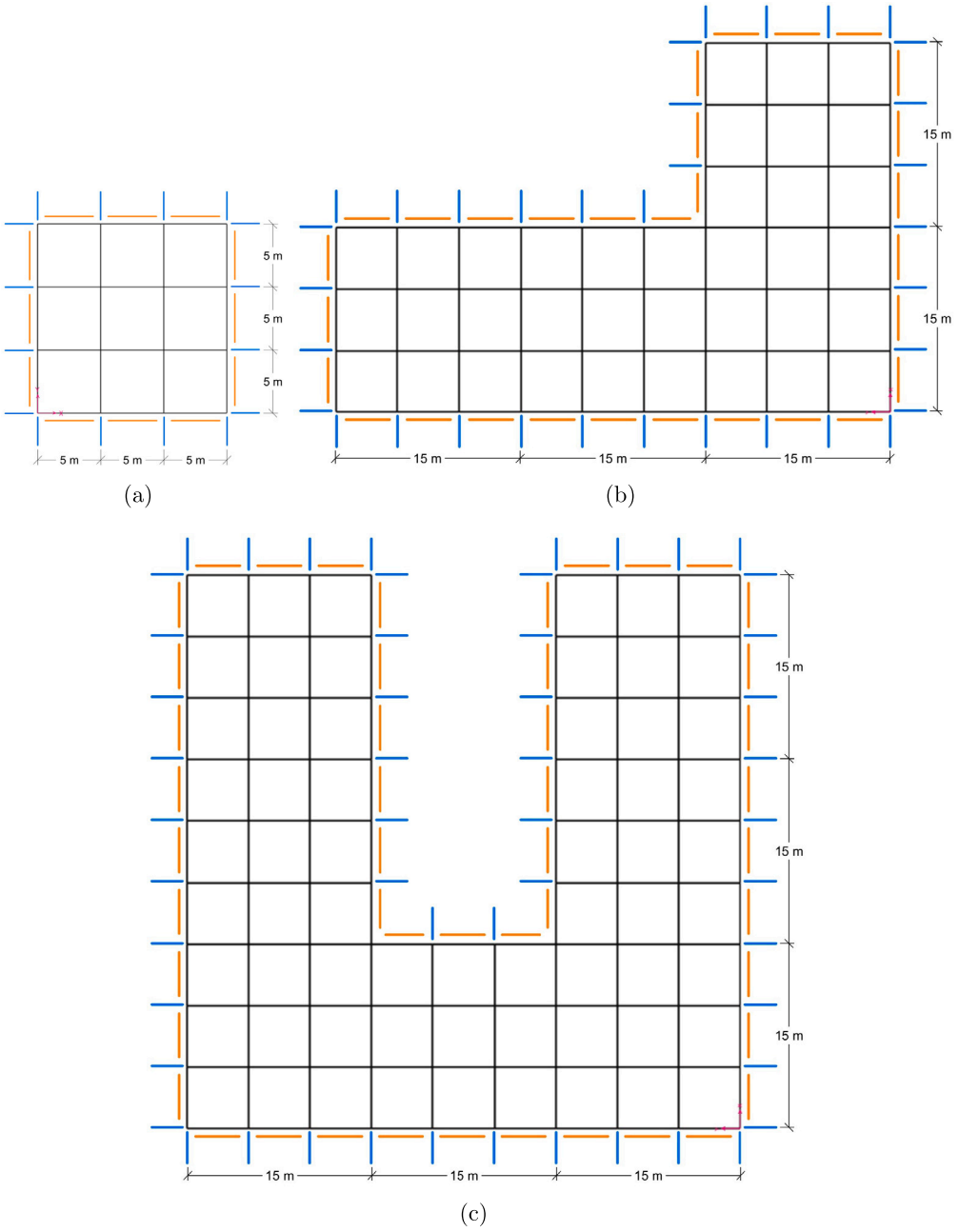

Fig. 5. Top view of the considered existing structures, square-shaped (a), L-shaped (b), U-shaped (c), with potential orthogonal (blue) and parallel (orange) exoskeletons.

Life Safety Limit State, with a corresponding peak ground acceleration a_g/g of 0.1337. All three buildings' fundamental frequencies correspond to the *plateau* of the response spectrum (0.42 g). The adopted elastic spectrum is shown and the fundamental periods corresponding to non-retrofitted solutions for all the investigated case studies are indicated in Fig. 6.

The choice of these seismic parameters is based on the need to investigate a situation where the seismic action is not trivial and can be representative of wide areas within the Mediterranean zone. Moreover all buildings start from almost the same position on the elastic spectrum to have a common seismic starting point in order to be able to compare the results of the retrofitting without starting bias. Furthermore, the introduction of exoskeletons increases the stiffness of the building, shifting the period downwards, therefore the chosen starting point allows to compare original and retrofitted building subjected to the same peak seismic action.

4. Results and discussion

Through the application of the optimization procedure detailed in Section 2 to the adopted Case Studies (Section 3), valuable insights have been gained. These are presented in this section and regard the performance of the employed algorithm, the characteristics of the final solution, and the effect of the exoskeletons on the structural behavior.

4.1. Performance of the algorithm

An efficient illustration of the algorithm's performance and evolution towards the final design is given by the plots of the Objective Function, Inter-storey Drift Ratio (ISDR) of the building, and Demand-Capacity Ratio (DCR) of the Exoskeletons, at each iteration. In Figs. 7(a)-(f), all these features have been reported for each case study. This kind of representation allows to appreciate the evolution strat-

Table 3
Summary of the steel weight of the exoskeletons (exosk.), the seismic mass of the unretrofitted structure, the weight of exosk. steel per unit area of the building (incidence), the maximum inter-storey drift ratio (ISDR) of the retrofitted structure and the maximum Demand-Capacity Ratio (DCR) of the exoskeleton elements, for each Case Study (CS#).

	CS 1	CS 2	CS 3	CS 4	CS 5	CS 6
exosk. weight [ton]	20.7	9.5	116.5	28.3	228.7	39.6
seismic mass [ton]	796.2	796.2	2942.3	2942.3	5071.8	5071.8
incidence [kg/m^2]	30.7	14.1	43.1	10.5	48.4	8.4
max ISDR of the str. [%]	99.95	98.52	99.98	99.45	99.98	99.55
max DCR of exosk. [%]	97.37	98.74	69.16	94.76	68.83	97.16

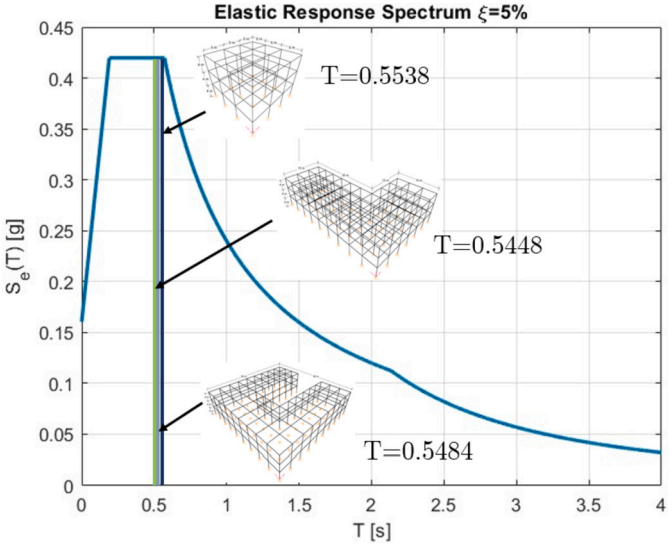

Fig. 6. Elastic response spectrum of Foggia, Italy.

egy followed by the optimizer. As expected, at each plot the OF trend rapidly converges to the near-optimal solution before approaching the maximum iteration. Further refinement can be addressed to the sizing capacity of the exoskeletons' members with gradually less evident mass-saving upgrades of the solution.

With specific regard to the evolution of the imposed constraints, the ISDR and DCR trends are more discontinuous with positive and negative jumps along the iteration. It can be appreciated that the evolution of the solution is towards maximizing both values while the weight is reduced. Nevertheless, it is noteworthy that the optimization tool primarily targets the maximum inter-storey drift. In other words, it represents the most critical constraints to be satisfied towards the achievement of the optimal design. As proof of this, especially for Fig. 7(c)-(e), the optimal design has been achieved by exploiting just 70% of the maximum strength of the most critical element while the maximum inter-storey drift approaches 100% of the allowable threshold. Hence, the oversizing of the exoskeletons is mainly caused by the satisfaction of the inter-storey drift constraint.

4.2. Optimal arrangement of the exoskeletons

In Fig. 8, the configuration of the final solution is shown for each case study, depicting the number and placement of exoskeletons resulting from the binary design variables. Additionally, the steel weight of each solution, along with the weight of the structure and the weight of exoskeleton steel per square meter of floor surface are presented in Table 3.

Giving a physical justification of the exoskeleton positions' strategy adopted by the optimizer, for each final configuration, plays a crucial role in the assessment of the results' reliability. Two main principles can be established, based on the observation of the final optimal arrangements.

The first principle is related to the distance between the center of mass (CM) and the center of stiffness (CK) of the building. Steel exoskeletons add more stiffness than mass to the system with respect to the existing structure's elements. Hence, even though introducing an exoskeleton changes the position of both CM and CK, the impact on the latter is more significant, allowing, if appropriately positioned, to reduce the eccentricity of seismic forces acting on the building. It is worth noticing how, for all three case studies, CM and CK are already reasonably close. Therefore, the exoskeletons have to keep this condition or improve it. It can be therefore achieved when the exoskeletons are positioned symmetric to CK.

The second main principle driving the positioning of exoskeletons is connected to the first one, and it is related to the displacement control. The optimal positions depend on the torsional behavior of the structure, since it can be subjected to rotational effects when CM and CK are non-coincident. In that case, exoskeletons positioning allows to make them coincident or, at least, closer, in order to mitigate torsional effects in the structural system. In this way, if the building displacements present a torsional component, the nodes that are farthest from CK are those ones subjected to the largest displacements. Thus, the exoskeletons positioned in such higher displacements regions are those ones that generate response forces with the largest arms, being therefore the most efficient to control this kind of torsional effect. On the other hand, if there is no torsional behavior in the building's response, exoskeletons positioned either far or close to CK provide the same displacement control. It is important to consider that, in this last case, exoskeletons positioned far from CK should be symmetrical to not introduce new eccentricities.

As a result, exoskeletons can be located in three ways. First, they can be placed far from CK and asymmetric to it, in case the design need is to modify the position of CK to bring it closer to CM to reduce eccentricity and, thus, control displacements' components originated from the torsional behavior. Second, they can be positioned away from CK but symmetric to it, which is useful to maintain the position of CK with respect to CM. Third, they can be positioned close to CK, which is useful for controlling translational components when the position of CK relative to CM does not need to be changed, i.e. the eccentricity is already minimal and therefore there is no torsional behavior to control. Finally, it is worth noting that the final configuration can consist of a combination of the above options. For example, an optimal configuration can combine exoskeletons positioned away from CK, to improve the torsional stiffness of the system and reduce its torsional modes, with some exoskeletons however positioned near the new position of CK, to control the translation component exclusively.

4.3. Cross-sections of the elements

The Circular Hollow Sections chosen for the exoskeleton members are listed in Table 4 for each case study. They correspond to the cross-

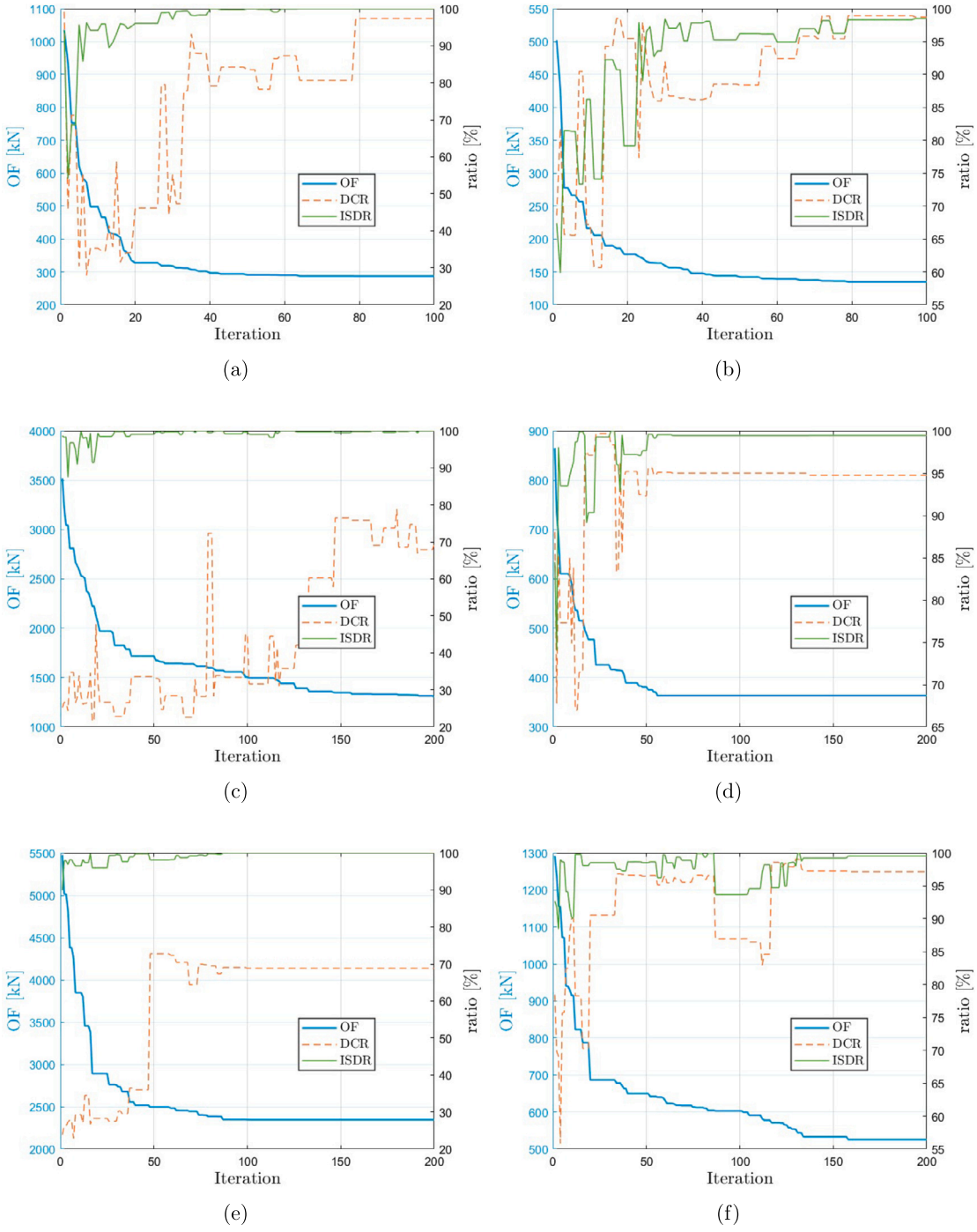

Fig. 7. Evolution of the Objective Function (OF), maximum Demand-Capacity Ratio (DCR), and maximum Inter-Storey Drift Ratio (ISDR) in the optimization, for each Case Study (CS#).

sectional property values assumed by the last four design variables coherently to the definition of the design vector.

The corresponding element to each design variable is indicated in Fig. 4. Case studies 1, 3, and 5 correspond to orthogonal exoskeletons, while 2, 4, and 6 to parallel ones. It can be appreciated from the results how the larger cross-sections are assigned to x_2 and x_3 (external vertical columns) for the orthogonal layout. For parallel exoskeletons, the larger cross-sections are assigned to the braces, represented by x_5, x_6, and x_7. As expected, the different orientations of the two exoskeleton configurations lead to different in-plane structural behavior of the external trusses.

4.4. Displacements

The introduction of a maximum allowable inter-storey drift as a constraint of the optimization lead to a significant control of these values. The floor displacements before and after the retrofit are presented in Fig. 9 for each case study. Reductions between 55 and 65% can be appreciated. A further improvement provided by the exoskeletons is the homogenization of the distribution of the inter-storey drifts that gain linear trends after retrofitting. This result is the direct output of the strategy of the optimizer which aims to satisfy the displacement constraint by equally distributing the inter-storey drifts among floors.

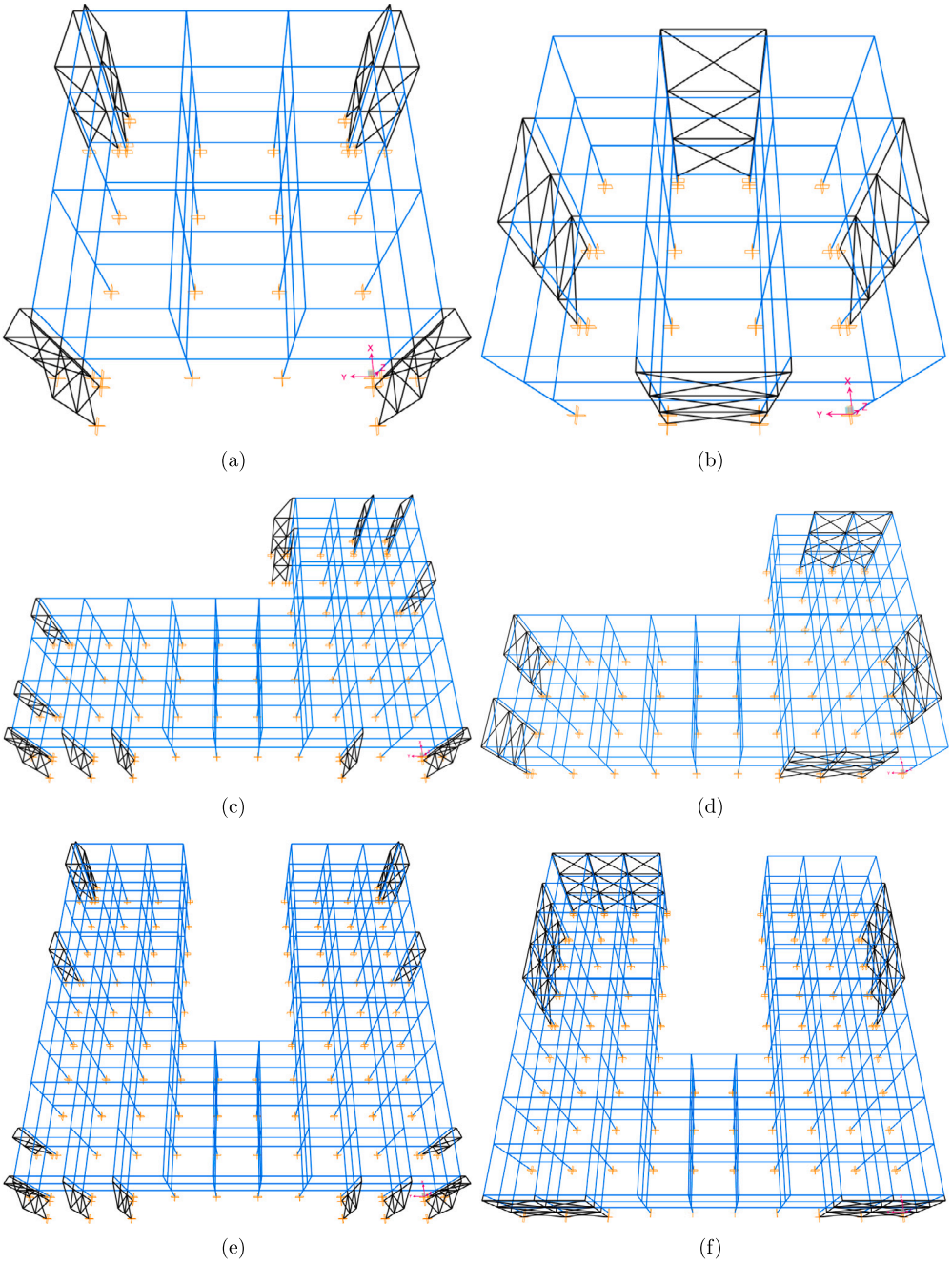

Fig. 8. Optimal exoskeleton configuration for each Case Study (CS#). Figs. (a)-(c)-(e) refer to case studies 1-3-5 while Figs. (b)-(d)-(f) to case studies 2-4-6.

4.5. Base-shears

Another main improvement in the seismic behavior resulting from the introduction of the retrofitting system is related to the base shear. As depicted in Fig. 10, the overall base shear is not significantly modified after the introduction of the retrofitting system. This is because the added mass from the exoskeletons is almost negligible compared to the mass of the structure. Furthermore, the periods of high-order modes of the retrofitted structures lie on the *plateau* of the response spectrum exactly as the ones of the original structures. This behavior was intentionally chosen by the authors to allow an easier comparison of the retrofitting efficiency keeping constant the external action.

As a conclusion, between 40 and 59% of the seismic force is sustained by the exoskeletons, thereby, resulting in all the buildings being significantly unloaded.

4.6. Structural verification of the building

The maximum allowable inter-storey drift has been selected as the threshold that guarantees the structural safety of the non-structural infills, maintaining theoretically the entire existing structure in the elastic range. Meanwhile, the structural elements of the buildings are significantly unloaded thanks to the extra-stiffness contribution provided by the exoskeletons.

The structural verifications of each element of the existing RC buildings have been conducted according to Italian Standard NTC18 [21]. The outputs are presented in Table 5 in terms of the percentage of non-verified elements and Demand-Capacity ratios of the most critical column and beam, before and after the retrofitting. Additionally, in Appendix A, color map illustrations of the structural verification after the seismic retrofit have been reported, for each case study.

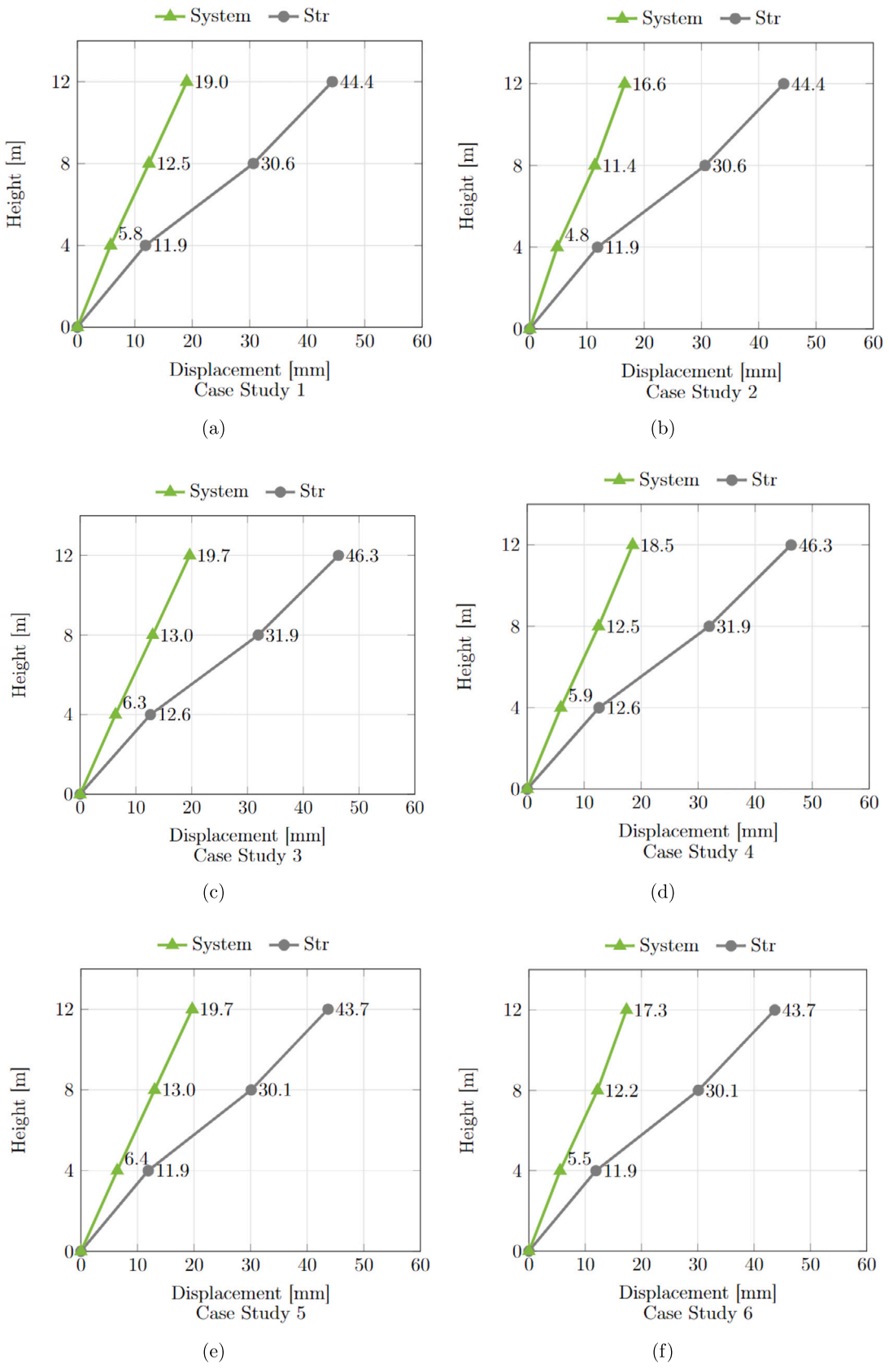

Fig. 9. Floor displacements before (Str) and after (System) the retrofitting intervention for each Case Study (CS#).

Table 4
CHS profiles of the exoskeleton's elements selected through the optimization process for each Case Study (CS#). Diameter (⌀) and thickness (t) are expressed in mm.

		CS1	CS2	CS3	CS4	CS5	CS6
x_1	⌀	101.6	177.8	193.7	244.5	406.4	244.5
	t	5	10	14.2	10	30	10
x_2	⌀	355.6	101.6	762.0	101.6	762.0	101.6
	t	25	5	40	5	50	5
x_3	⌀	323.9	101.6	406.4	101.6	610.0	101.6
	t	14.2	5	40	5	40	5
x_4	⌀	114.3	101.6	168.3	101.6	177.8	101.6
	t	6.3	5	8	5	10	5
x_5	⌀	139.7	177.8	219.1	244.5	244.5	244.5
	t	8	10	10	10	14.2	10
x_6	⌀	193.7	177.8	323.9	273.0	406.4	219.1
	t	14.2	10	20	16	30	14.2
x_7	⌀	177.8	139.7	323.9	177.8	457.0	177.8
	t	10	8	25	10	30	10
x_8	⌀	406.4	323.9	762.0	406.4	762.0	406.4
	t	14.2	14.2	25	14.2	25	14.2

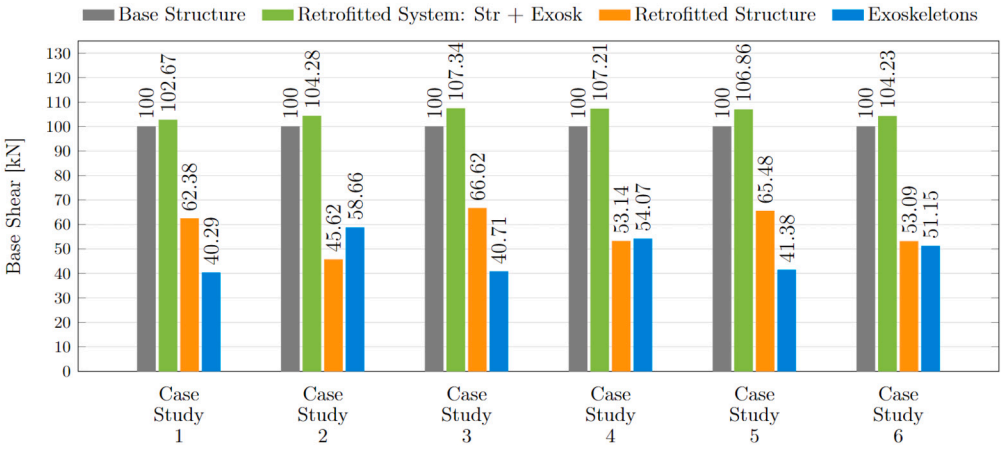

Fig. 10. Total base-shear in X-direction of the retrofitted system (building and exoskeletons) (System), the building after the retrofit (System-Str), and the exoskeletons (System-Exosk), in comparison to the one of the existing structure before the retrofit (Str).

Table 5
Results of the structural verifications of the existing buildings, in terms of percentage of non-verified elements and Demand-Capacity ratios of the most critical column and beam, before and after the retrofit, for each Case Study (CS#).

		% Non-verif. elements	Max DCR col	Max DCR beam
Square-shaped	Before retrofitting	83.33	1.939	2.082
	Orthogonal exosk.: **CS1**	10.00	1.606	0.980
	Parallel exosk.: **CS2**	3.33	0.948	1.003
L-shaped	Before retrofitting	79.14	2.154	1.961
	Orthogonal exosk.: **CS3**	10.07	0.928	2.516
	Parallel exosk.: **CS4**	7.91	1.542	1.070
U-shaped	Before retrofitting	78.99	2.114	2.081
	Orthogonal exosk.: **CS5**	7.28	2.706	1.130
	Parallel exosk. **CS6**	7.42	1.471	1.121

Analyzing the aforementioned results, it can be appreciated how the proposed intervention, designed by fixing a maximum allowable inter-storey drift, can significantly reduce the number of elements that do not satisfy the structural verification, in compliance with the adopted standard regulation.

Starting from the *Squared-shaped* building up to the *U-shape* building the percentage of non-verified elements significantly reduces from approximately 80% to values lower than 10%. It is worth noting that the proposed method ensures that the displacement constraints (i.e. inter-storey drift) are satisfied even if no guarantee can be assured for the

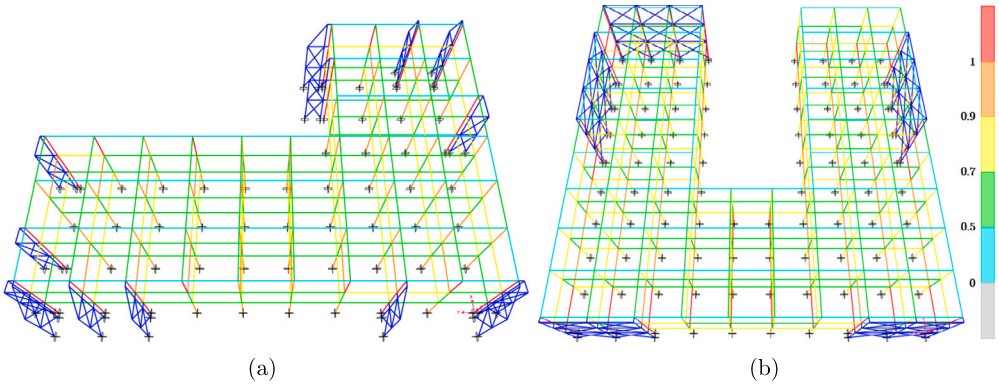

Fig. 11. Color map of the structural verifications performed on the retrofitted structures according to the Italian Regulation NTC2018 for Case Studies 3 (a) and 6 (b). According to the legend, overstressed elements (DCR higher than 1) have been depicted in red color.

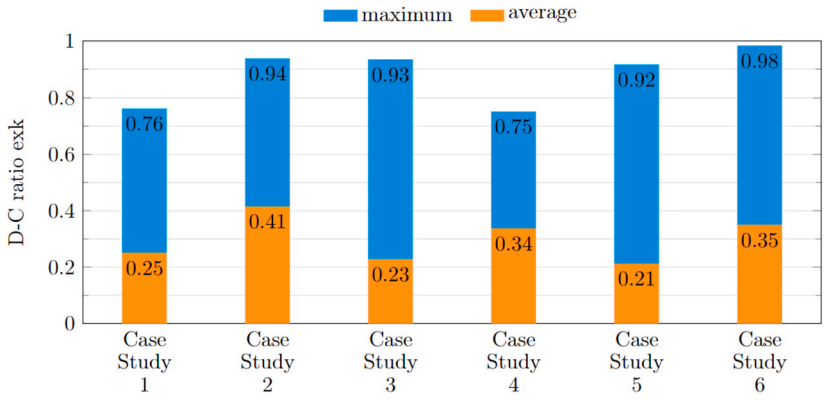

Fig. 12. Maximum Demand-Capacity Ratio of the most critical exoskeleton element (maximum) and average among all exoskeleton elements (average), for each Case Study (CS#).

structural safety of the element composing the existing structure. It stands to reason that the so strict displacement constraints should have ensured a significant unloading of the base structure resulting in an easy verification of its inner elements. Among all the verification outputs of all case studies reported in Appendix A, color map visualization, provided by *SAP2000*, of CS3 with orthogonal exoskeletons (see Fig. 11-a) and CS6 with parallel ones (see Fig. 11-b) have been selected for further considerations.

As observed in all the investigated case studies, columns directly connected to the exoskeletons as well as some of the surrounding beams suffer from a concentration of stresses caused by the transfer of forces from the building to the exoskeletons. During the assembling of the exoskeletons, all these elements need local interventions aiming to guarantee an appropriate level of strength and stiffness. However, by observing the color map illustrations depicted in Fig. 11a-b, it is clear that elements of the existing structure located far from the external strengthening system exhibit high values of DCR. In fact, the unloading effect provided by the exoskeletons leads to acceptable results, even if some columns and beams lying on the last floor of the L-shape and U-shape buildings, still remain close to the maximum safety threshold with DCR close to 1 or even a little higher.

In these specific cases, local intervention inside the building should be provided to guarantee the safety of all the structural elements composing the existing structure.

As a consequence, the structural safety of the existing structure must be verified case-by-case. However, the benefits of adopting exoskeleton systems for seismic retrofitting in comparison with traditional retrofitting techniques still remain unquestionable as testified by the reduction of the overstressed elements reported in Table 5.

4.7. Demand-capacity ratios of the exoskeletons

An interesting comparison between the two layouts (orthogonal and parallel) can be performed with reference to the Demand-Capacity ratios (DCRs) of the exoskeletons elements. In Fig. 12, a comparison between the average DCR considering all exoskeleton's elements, and the maximum one, thus, the one corresponding to the most critical element of the retrofitting system, is performed.

It can be observed that when the average value is close to the maximum one the forces are better distributed within the exoskeletons. Therefore, parallel exoskeletons achieve the same control over the structural response of the building with a lower weight because their elements are more uniformly stressed. However, significant difference between the maximum Demand-Capacity Ratio and the average one still appear after the optimization in all the case studies. This result proves that controlling inter-storey drift rather than maximizing the retrofitting elements structural performance does not lead to the minimum steel weight configuration, as it can be seen in Fig. 7.

Moreover it is noteworthy that the inclination of the braces has a significant effect on their effectiveness, and consequently, on the stress distribution among the exoskeleton's elements. The geometry of the parallel exoskeletons is given by the length of the building's module (5 m) and by the floor height (4 m), resulting in an inclination angle of the bracings of 38.65°. On the other hand, perpendicular exoskeletons' geometry is defined by the free space around the building in which the exoskeletons can be placed (2.5 m), and the floor height (4 m) as well, resulting in an inclination angle of the bracings of 63.43°.

It has been proven that the closer the inclination angle is to 45°, the more effective the bracings [67], and that this angle should be maintained between 30 and 60°.

In conclusion, for these specific geometries, parallel exoskeletons are more efficient than perpendicular ones, but this behavior may be strongly dependent on the building's characteristics, which define the exoskeletons' geometry and, therefore, the inclination of the bracings.

5. Conclusions

In this study, an optimization procedure based on an adapted Genetic Algorithm has been proposed for the design of an exoskeleton solution for the seismic protection of buildings. By implementing this procedure, it is possible to determine the optimal number and position of exoskeletons, as well as the cross-sections of their constitutive elements.

The optimization procedure has been applied to six case studies given by existing Reinforced Concrete structures with Demand-Capacity Ratios around 2, in a large number of elements: columns and beams. Two different two-dimensional exoskeleton layouts are studied for the retrofit of each building, which are orthogonal and parallel to its façade.

Despite the criticality of the case studies, the structural behavior has been successfully controlled, demonstrating the effectiveness of exoskeletons as a retrofitting method. The intervention achieved an average reduction of the maximum inter-storey drift of 65%, in addition to a base shear reductions between 40% and 60%. Furthermore, by imposing a maximum inter-storey drift, a significant improvement in the building's elements condition was achieved, in terms of seismic structural verification, as after the retrofit only some columns connected to the exoskeletons require local intervention.

The assessment of two different layouts, with exoskeleton components orthogonal and parallel to the building façade, allowed a more in-depth study of the differences in their behavior. In particular, the distribution of stresses in the parallel exoskeletons' elements is more uniform than for the orthogonal exoskeletons. Therefore, a solution with parallel exoskeletons can achieve the same level of improvement while being significantly lighter, for the inclination of the bracings considered in this study.

Additionally, the analysis of the final arrangement of the exoskeletons around the buildings' perimeters provided interesting insights into the characteristics of the preferred configurations. Two principles were identified, which represent a practical guideline for the design of the arrangement of an intervention with exoskeletons.

Moreover, by applying the proposed procedure to existing structures of different complexity and irregularity, the effectiveness and robustness of the algorithm, to find the solution that minimizes the weight while meeting the established targets, has been verified. Finally, as a future development of this study, it would be interesting to explore three-dimensional configurations of exoskeletons, as well as the application to a more complex case study as tall buildings with irregularities in height.

CRediT authorship contribution statement

Jana Olivo: Writing – review & editing, Writing – original draft, Visualization, Software, Methodology, Investigation, Formal analysis, Data curation, Conceptualization. **Raffaele Cucuzza:** Writing – review & editing, Writing – original draft, Visualization, Validation, Supervision, Software, Project administration, Methodology, Investigation, Funding acquisition, Formal analysis, Data curation, Conceptualization. **Gabriele Bertagnoli:** Writing – review & editing, Validation, Supervision, Methodology, Investigation, Data curation. **Marco Domaneschi:** Writing – review & editing, Writing – original draft, Visualization, Supervision.

Declaration of competing interest

The authors declare that they have no known competing financial interests or personal relationships that could have appeared to influence the work reported in this paper.

Data availability

Data will be made available on request.

Acknowledgements

The research leading to these results has received funding from the European Research Council under the Grant agreement ID: 101007595 of the project ADDOPTML, MSCA RISE 2020 Marie Skodowska Curie Research and Innovation Staff Exchange (RISE). This study was partially developed within the research activities carried out in the framework of the 2022-2024 ReLUIS Project—WP5.1 (Coordinators — G.A. Ferro, R. Cucuzza).

Appendix A

In this appendix, the color map outputs obtained from *SAP200*, by performing structural verifications on the retrofitted structures accord-

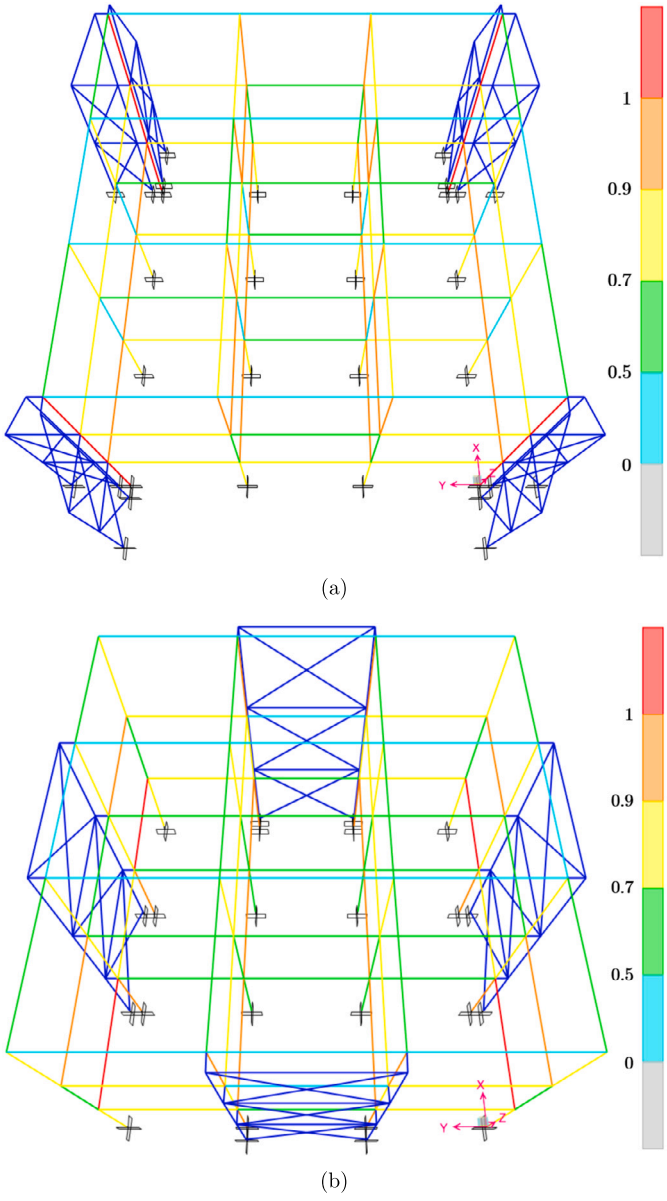

Fig. A.13. Color map of the structural verifications performed on the retrofitted structures according to the Italian Regulation NTC2018 for the square-shaped building, corresponding to Case Studies 1 (a) and 2 (b). According to the legend, overstressed elements (DCR higher than 1) have been depicted in red color.

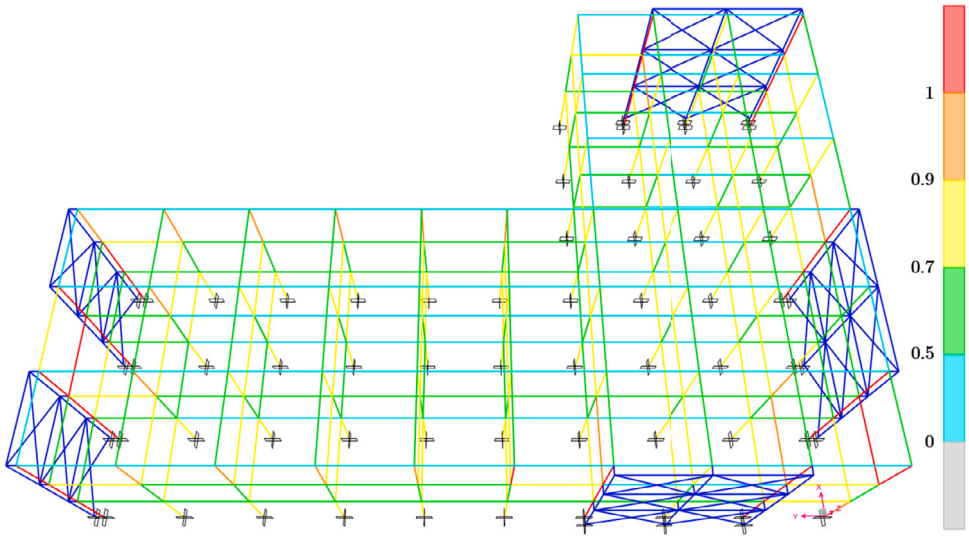

(a)

Fig. A.14. Color map of the structural verifications performed on the retrofitted structures according to the Italian Regulation NTC2018 for the L-shaped building, corresponding to the Case Study 4. According to the legend, overstressed elements (DCR higher than 1) have been depicted in red color.

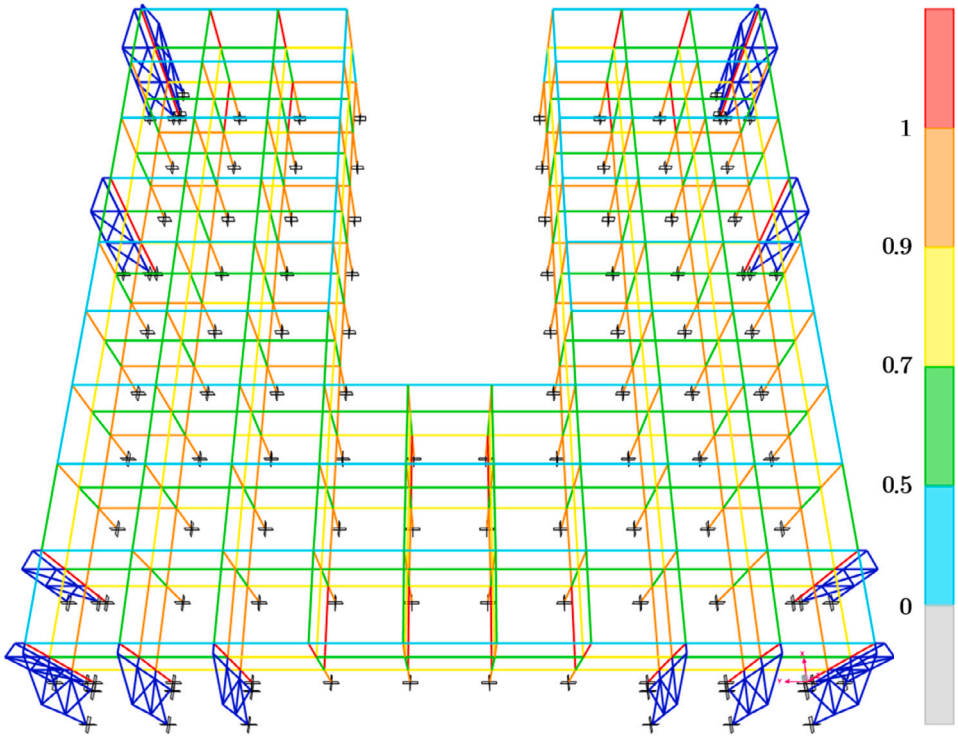

(a)

Fig. A.15. Color map of the structural verifications performed on the retrofitted structures according to the Italian Regulation NTC2018 for the U-shaped building, corresponding to the Case Study 5. According to the legend, overstressed elements (DCR higher than 1) have been depicted in red color.

ing to the Italian Regulation NTC2018, have been introduced for each Case Study (Figs. A.13, A.14 and A.15).

References

[1] Kelam AA, Karimzadeh S, Yousefibavil K, Akgün H, Askan A, Erberik MA, et al. An evaluation of seismic hazard and potential damage in gaziantep, Turkey using site specific models for sources, velocity structure and building stock. Soil Dyn Earthq Eng 2022;154:107129.

[2] Foraboschi P. Versatility of steel in correcting construction deficiencies and in seismic retrofitting of rc buildings. J Build Eng 2016;8:107–22.

[3] Crowley H, Dabbeek J, Despotaki V, Rodrigues D, Martins L, Silva V, et al. European seismic risk model (esrm20). EFEHR Technical Report 2. 2021.

[4] Corbane C, Hancilar U, Ehrlich D, De Groeve T. Pan-European seismic risk assessment: a proof of concept using the earthquake loss estimation routine (eler). Bull Earthq Eng 2017;15:1057–83.

[5] Belleri A, Marini A. Does seismic risk affect the environmental impact of existing buildings? Energy Build 2016;110:149–58.

[6] D'Urso S, Cicero B. From the efficiency of nature to parametric design. A holistic approach for sustainable building renovation in seismic regions. Sustainability 2019;11(5):1227.

[7] Passoni C, Guo J, Christopoulos C, Marini A, Riva P. Design of dissipative and elastic high-strength exoskeleton solutions for sustainable seismic upgrades of existing rc buildings. Eng Struct 2020;221:111057.

[8] Building Performance Institute Europe (BPIE), Europe's buildings under the microscope: a country-by-country review of the energy performance of the buildings. Brussels; 2011.

[9] Domaneschi M, Cucuzza R, Martinelli L, Noori M. Service-life extension of transport infrastructure through structural health monitoring. In: Life-cycle of structures and infrastructure systems. CRC Press; 2023. p. 4131–8.

[10] Martinelli L, Domaneschi M, Cucuzza R, Noori M. Service-life extension of transport infrastructure through structural control. In: Life-cycle of structures and infrastructure systems. CRC Press; 2023. p. 4139–46.

[11] Domaneschi M, Cucuzza R. Structural resilience through structural health monitoring: a critical review. In: Data driven methods for civil structural health monitoring and resilience; 2024. p. 1–13.

[12] Domaneschi M, Cucuzza R, Martinelli L, Noori M, Marano GC. A probabilistic framework for the resilience assessment of transport infrastructure systems via structural health monitoring and control based on a cost function approach. In: Structure and infrastructure engineering; 2024. p. 1–13.

[13] Rosso MM, Cucuzza R, Marano GC, Aloisio A, Cirrincione G. Review on deep learning in structural health monitoring. In: Bridge safety, maintenance, management, life-cycle, resilience and sustainability. CRC Press; 2022. p. 309–15.

[14] Passoni C, Marini A, Belleri A, Menna C. A multi-step design framework based on life cycle thinking for the holistic renovation of the existing buildings stock. IOP conference series: Earth and environmental science, vol. 290. IOP Publishing; 2019. p. 012134.

[15] Gkournelos P, Triantafillou T, Bournas D. Seismic upgrading of existing masonry structures: a state-of-the-art review. Soil Dyn Earthq Eng 2022;161. https://doi.org/10.1016/j.soildyn.2022.107428.

[16] Ong C-B, Chin C-L, Ma C-K, Tan J-Y, Awang AZ, Omar W. Seismic retrofit of reinforced concrete beam-column joints using various confinement techniques: a review. Structures 2022;42:221–43. https://doi.org/10.1016/j.istruc.2022.05.114.

[17] Soong T, Spencer Jr B. Supplemental energy dissipation: state-of-the-art and state-of-the-practice. Eng Struct 2002;24(3):243–59. https://doi.org/10.1016/S0141-0296(01)00092-X.

[18] Ikeda Y. Active and semi-active vibration control of buildings in Japan-practical applications and verification. Struct Control Health Monit 2009;16(7–8):703–23. https://doi.org/10.1002/stc.315.

[19] Spencer Jr B, Nagarajaiah S. State of the art of structural control. J Struct Eng 2003;129(7):845–56. https://doi.org/10.1061/(ASCE)0733-9445(2003)129:7(845).

[20] Medeot R, Zordan T. Development and revision of the European standard en 15129 on anti-seismic devices. In: Life-cycle civil engineering: innovation, theory and practice. CRC Press; 2021. p. 600–8.

[21] DM17/01/2018, Aggiornamento delle "Norme tecniche per le costruzioni". In: Italian ministry of infrastructures and transportation; 2018 (in Italian).

[22] Reggio A, Restuccia L, Martelli L, Ferro GA. Seismic performance of exoskeleton structures. Eng Struct 2019;198:109459. https://doi.org/10.1016/j.engstruct.2019.109459.

[23] Di Lorenzo G, Colacurcio E, Di Filippo A, Formisano A, Massimilla A, Landolfo R. State-of-the-art on steel exoskeletons for seismic retrofit of existing rc buildings. Int J 2020;37(1-2020).

[24] Benyus JM. Biomimicry: innovation inspired by nature. New York: Morrow; 1997.

[25] Pohl G, Nachtigall W. Biomimetics for architecture & design: nature-analogies-technology. Springer; 2015.

[26] A. S. of Civil Engineers, Civil engineers, minimum design loads for buildings and other structures. American Society of Civil Engineers; 2013.

[27] Reggio A, Greco R, Marano GC, Ferro GA. Stochastic multi-objective optimisation of exoskeleton structures. J Optim Theory Appl 2020;187:822–41.

[28] Cucuzza R, Aloisio A, Domaneschi M, Nascimbene R. Multimodal seismic assessment of infrastructures retrofitted with exoskeletons: insights from the foggia airport case study. In: Bullettin of earthquake engineering; 2024.

[29] Mazza F. Dissipative steel exoskeletons for the seismic control of reinforced concrete framed buildings. Struct Control Health Monit 2021;28(3):e2683.

[30] Domaneschi M. Simulation of controlled hysteresis by the semi-active bouc-wen model. Comput Struct 2012;106:245–57.

[31] Cucuzza R, Domaneschi M, Greco R, Marano GC. Numerical models comparison for fluid-viscous dampers: performance investigations through genetic algorithm. Comput Struct 2023;288:107122.

[32] Caverzan A, Lamperti Tornaghi M, Negro P. Roadmap for the improvement of earthquake resistance and eco-efficiency of existing buildings and cities. In: Proceedings of SAFESUST workshop, JRC. Ispra, Italy: JRC Science Hub; 2015. p. 1–136.

[33] Feroldi F, Marini A, Belleri A, Passoni C, Riva P, Preti M, et al. Miglioramento e adeguamento sismico di edifici contemporanei mediante approccio integrato energetico, architettonico e strutturale con soluzioni a doppio involucro a minimo impatto ambientale. Progett Sism 2014;2 (in Italian).

[34] Marini A, Passoni C, Riva P, Negro P, Romano E, Taucer F, et al. Technology options for earthquake resistant, eco-efficient buildings in Europe: research needs. In: European commission, joint research centre scientific and policy reports; 2014.

[35] Marini A, Belleri A, Feroldi F, Passoni C, Preti M, Riva P, et al. Coupling energy refurbishment with structural strengthening in retrofit interventions. In: SAFESUST workshop, SAFESUST Ispra; 2015. p. 26–7.

[36] Passoni C. Holistic renovation of existing rc buildings: a framework for possible integrated structural interventions. Ph.D. thesis. University of Brescia; 2016.

[37] Caverzan A, Lamperti Tornaghi M, Negro P. Taxonomy of the redevelopment methods for non-listed architecture: from façade refurbishment to the exoskeleton system. In: JRC, conference and workshop reports, proceedings of safesust workshop; November 2016. p. 26–7.

[38] Marini A, Passoni C, Belleri A, Feroldi F, Preti M, Metelli G, et al. Combining seismic retrofit with energy refurbishment for the sustainable renovation of rc buildings: a proof of concept. Eur J Environ Civ Eng 2022;26(7):2475–95.

[39] Cucuzza R, Domaneschi M, Rosso MM, Martinelli L, Marano GC. Cutting stock problem (csp) applied to structural optimization for the minimum waste cost. ce/Papers 2023;6(5):1066–73.

[40] Labò S, Passoni C, Marini A, Belleri A. Design of diagrid exoskeletons for the retrofit of existing rc buildings. Eng Struct 2020;220:110899.

[41] Martelli L, Restuccia L, Ferro G. The exoskeleton: a solution for seismic retrofitting of existing buildings. Proc Struct Integ 2020;25:294–304.

[42] European Committee for Standardization (CEN), Design of structures for earthquake resistance, Brussels, Belgium, 2005.

[43] Reggio A, Restuccia L, Martelli L, Ferro GA. Seismic performance of exoskeleton structures. Eng Struct 2019;198:109459.

[44] Di Lorenzo G, Tartaglia R, Prota A, Landolfo R. Design procedure for orthogonal steel exoskeleton structures for seismic strengthening. Eng Struct 2023;275:115252.

[45] Ciampi V, De Angelis M, Paolacci F. Design of yielding or friction-based dissipative bracings for seismic protection of buildings. Eng Struct 1995;17(5):381–91.

[46] Rosso M, Melchiorre J, Cucuzza R, Manuello A, Marano G, et al. Estimation of distribution algorithm for constrained optimization in structural design. In: Pursuing the infinite potential of computational mechanics, international centre for numerical methods in engineering. CIMNE; 2022.

[47] Habashneh M, Cucuzza R, Domaneschi M, Rad MM. Advanced elasto-plastic topology optimization of steel beams under elevated temperatures. Adv Eng Softw 2024;190:103596.

[48] Rosso MM, Cucuzza R, Aloisio A, Marano GC. Enhanced multi-strategy particle swarm optimization for constrained problems with an evolutionary-strategies-based unfeasible local search operator. Appl Sci 2022;12(5):2285.

[49] Rosso MM, Cucuzza R, Di Trapani F, Marano GC. Nonpenalty machine learning constraint handling using pso-svm for structural optimization. Adv Civ Eng 2021;2021:1–17.

[50] Bertagnoli G, Giordano L, Mancini S. Optimization of concrete shells using genetic algorithms. J Appl Math Mech/Z Angew Math Mech 2014;94(1–2):43–54.

[51] Cucuzza R, Costi C, Rosso MM, Domaneschi M, Marano GC, Masera D. Optimal strengthening by steel truss arches in prestressed girder bridges. In: Proceedings of the institution of civil engineers-bridge engineering. Thomas Telford Ltd; 2021. p. 1–21.

[52] Cucuzza R, Rosso MM, Aloisio A, Melchiorre J, Giudice ML, Marano GC. Size and shape optimization of a guyed mast structure under wind, ice and seismic loading. Appl Sci 2022;12(10):4875.

[53] Kashani AR, Camp CV, Rostamian M, Azizi K, Gandomi AH. Population-based optimization in structural engineering: a review. Artif Intell Rev 2022:1–108.

[54] Blum C, Roli A. Metaheuristics in combinatorial optimization: overview and conceptual comparison. ACM Comput Surv 2003;35(3):268–308.

[55] Gandomi AH, Yang X-S, Talatahari S, Alavi AH. Metaheuristic applications in structures and infrastructures. Newnes 2013.

[56] Holland J. Adaptation in natural and artificial systems; 1975.

[57] Ghobarah A. On drift limits associated with different damage levels. In: International workshop on performance-based seismic design, vol. 28. Canada: Department of Civil Engineering, McMaster University Ontario; 2004.

[58] Jiang H, Fu B, Chen L. Damage-control seismic design of moment-resisting rc frame buildings. J Asian Archit Build Eng 2013;12(1):49–56.

[59] EN1993-1-1, Eurocode 3: design of steel structures - part 1-1: general rules and rules for buildings. Brussels, Belgium: The European Union per Regulation; 2005.

[60] Mitchell M. Genetic algorithms: an overview. Complexity 1995;1(1):31–9.

[61] Beaslev D, Bull DR, Martin RR. An overview of genetic algorithms: part 2, research topics. Univ Comput 1993;15(4).

[62] Tomassini M. A survey of genetic algorithms. Ann Revf Comput Phys III 1995:87–118.

[63] Beasley D, Bull DR, Martin RR. An overview of genetic algorithms: part 1, fundamentals. Univ Comput 1993;15(2):56–69.

[64] EN1998-1, Eurocode 8: design of structures for earthquake resistance – part 1: general rules, seismic actions and rules for buildings. Brussels, Belgium: The European Union per Regulation; 2004.

[65] CSI, Sap2000 integrated software for structural analysis and design; 2023.
[66] MATLAB, Version 9.0.3.713579 (R2017b). Natick, Massachusetts: The MathWorks Inc.; 2017.
[67] Lu H, Gilbert M, Tyas A. Theoretically optimal bracing for pre-existing building frames. Struct Multidiscip Optim 2018;58:677–86.